EBioMedicine 44 (2019) 194–208

Contents lists available at ScienceDirect

EBioMedicine

journal homepage: www.ebiomedicine.com

EBioMedicine
Published by THE LANCET

Research paper

# $Ca^{2+}$ and CACNA1H mediate targeted suppression of breast cancer brain metastasis by AM RF EMF

Sambad Sharma [a], Shih-Ying Wu [a], Hugo Jimenez [a], Fei Xing [a], Dongqin Zhu [a], Yin Liu [a], Kerui Wu [a], Abhishek Tyagi [a], Dan Zhao [a], Hui-Wen Lo [a], Linda Metheny-Barlow [b], Peiqing Sun [a], John D. Bourland [b], Michael D. Chan [b], Alexandra Thomas [c], Alexandre Barbault [d], Ralph B. D'Agostino [e], Christopher T. Whitlow [f], Volker Kirchner [g], Carl Blackman [a], Boris Pasche [a], Kounosuke Watabe [a,*]

[a] Department of Cancer Biology, Wake Forest Baptist Medical Center, Winston-Salem, NC, United States of America
[b] Department of Radiation Oncology, Wake Forest Baptist Medical Center, Winston-Salem, NC, United States of America
[c] Department of Hematology and Oncology, Wake Forest Baptist Medical Center, Winston-Salem, NC, United States of America
[d] TheraBionic GmbH, Ettlingen, Germany
[e] Department of Biostatistical Sciences, Division of Public Health Sciences, Wake Forest Baptist Medical Center, Winston-Salem, NC, United States of America
[f] Department of Radiology, Wake Forest Baptist Medical Center, Winston-Salem, NC, United States of America
[g] Genolier Cancer Center, Genolier, Switzerland

ARTICLE INFO

*Article history:*
Received 27 March 2019
Received in revised form 14 May 2019
Accepted 15 May 2019
Available online 23 May 2019

*Keywords:*
Breast Cancer
Brain metastasis
Electromagnetic field
Radiofrequency
Calcium
Novel therapeutics
Cav3.2 T-type channel
Exosomes
Radiation
miRNA
Angiogenesis

ABSTRACT

*Background*: Brain metastases are a major cause of death in patients with metastatic breast cancer. While surgical resection and radiation therapy are effective treatment modalities, the majority of patients will succumb from disease progression. We have developed a novel therapy for brain metastases that delivers athermal radiofrequency electromagnetic fields that are amplitude-modulated at breast cancer specific frequencies (BCF).
*Methods*: 27.12 MHz amplitude-modulated BCF were administered to a patient with a breast cancer brain metastasis by placing a spoon-shaped antenna on the anterior part of the tongue for three one-hour treatments every day. In preclinical models, a BCF dose, equivalent to that delivered to the patient's brain, was administered to animals implanted with either brain metastasis patient derived xenografts (PDXs) or brain-tropic cell lines. We also examined the efficacy of combining radiation therapy with BCF treatment. Additionally, the mechanistic underpinnings associated with cancer inhibition was identified using an agnostic approach.
*Findings*: Animal studies demonstrated a significant decrease in growth and metastases of brain-tropic cell lines. Moreover, BCF treatment of PDXs established from patients with brain metastases showed strong suppression of their growth ability. Importantly, BCF treatment led to significant and durable regression of brain metastasis of a patient with triple negative breast cancer. The tumour inhibitory effect was mediated by $Ca^{2+}$ influx in cancer cells through CACNA1H T-type voltage-gated calcium channels, which, acting as the cellular antenna for BCF, activated CAMKII/p38 MAPK signalling and inhibited cancer stem cells through suppression of β-catenin/HMGA2 signalling. Furthermore, BCF treatment downregulated exosomal miR-1246 level, which in turn decreased angiogenesis in brain environment. Therefore, targeted growth inhibition of breast cancer metastases was achieved through CACNA1H.
*Interpretation*: We demonstrate that BCF, as a single agent or in combination with radiation, is a novel treatment approach to the treatment of brain metastases. This paradigm shifting modality warrants further clinical trials for this unmet medical need.


## 1. Introduction

Brain metastasis is an emerging problem in oncology and there are >170,000 new cases in the US every year [1,2]. Breast cancer is the second leading cause of brain metastasis, and approximately 5–15% of patients with metastatic breast cancer will develop symptomatic brain metastasis [3–5]. Radiation therapy with stereotactic radiosurgery

DOI of original article: https://doi.org/10.1016/j.ebiom.2019.05.034.
* Corresponding author at: Department of Cancer Biology, Wake Forest University School of Medicine, Winston-Salem, NC 27157, Unites States of America
*E-mail address:* kwatabe@wakehealth.edu (K. Watabe).

https://doi.org/10.1016/j.ebiom.2019.05.038

**Research in context**

*Evidence before this story*

Our group has previously identified amplitude modulated radiofrequency electromagnetic fields (AM RF EMF) in patients diagnosed with multiple cancers. In a pilot study, we administered these frequencies to cancer patients in compassionate clinical trials, and observed both complete and partial responses in some patients with breast and hepatocellular cancer metastatic to multiple organs, thus demonstrating systemic antitumour effects of AM RF EMF. However, the underlying mechanism behind the response was unknown.

*Added value of this study*

We tested the hypothesis that this approach is effective in the treatment of brain metastasis of breast cancer patients. We examined the antitumour effect of breast cancer-specific AM RF EMF (BCF) in brain metastatic disease at the same Specific Absorption Rate (SAR) levels as those delivered to the patients. BCF suppressed the growth of two brain-metastatic breast cancer cell lines and two brain-metastatic PDXs. Additionally, BCF had long-lasting antitumour activity in a patient with breast cancer brain metastasis. We also discovered that combining radiation treatment with BCF resulted in increased treatment efficacy, suggesting that this novel treatment approach could enhance the effect of radiation therapy. We then studied the mechanism of action and found that BCF triggered calcium influx from the extracellular to the intracellular compartments through $Ca_V3.2$ voltage-gated calcium channels (CACNA1H), increasing calcium mediated Calmodulin-activated kinase II (CAMKII) dependent activation of p38 MAPK pathway leading to cell growth inhibition. Importantly, BCF suppressed the cancer stem cell properties of brain metastatic cells by decreasing HMGA2 gene expression. Activation of CAMKII by BCF phosphorylated and primed β-catenin for degradation thereby decreasing HMGA2 expression and cancer stem cell (CSC) population. Additionally, BCF reduced the level of miR-1246 in exosomes secreted by brain metastatic cells, which resulted in decreased angiogenesis in brain microenvironment.

*Implications of all the available evidence*

Our results demonstrate that BCF is a novel targeted treatment approach for breast cancer brain metastasis with minimum toxicity. Considering the efficacy and established safety profile of BCF, our results have strong implication in improving survival and quality of life of patients with brain metastasis.

and/or whole brain radiation therapy are considered effective treatments; however, most patients eventually experience disease recurrence [6]. Radiation therapy also often causes cognitive side effects which significantly dampen the quality of life [7]. Therefore, there is an unmet need for a novel therapeutic approach that can increase survival outcome of patients with brain metastasis.

The biological activity of athermal electromagnetic fields in cancer has been extensively studied and there are many controversial and contradictory findings [8,9]. Using non-invasive methods assessing changes in pulse pressure, we have previously reported the identification of tumour-specific modulation frequencies in patients with various forms of cancer [10]. We sought to determine if administration of RF EMF sinusoidally amplitude-modulated at tumour-specific frequencies by means of an emitting antenna placed in the patient's mouth could affect tumour growth. Such an approach results in a whole body averaged specific absorption rate (SAR) of 1.35 mW/kg, which is more than one hundred fold lower than the SAR generated by cellphones and does not result in heating of any body part and is well below the International Standards for Safety Exposure [11]. In our feasibility study treatment of breast cancer patients with RF EMF, which were amplitude-modulated at breast cancer-specific frequencies, resulted in both complete and partial responses in patients with stage IV metastatic disease. Objective tumour shrinkage was documented in bone and adrenal gland, thus demonstrating systemic antitumour effects of BCF [10]. Importantly, this treatment has been shown to be minimally invasive, low risk, well tolerated and yields tumour shrinkage in patients with metastatic breast cancer. In July 2018, the TheraBionic P1 medical device emitting hepatocellular carcinoma-specific AM RF EMF received European regulatory approval as a class IIa, low risk systemic treatment for patients with advanced hepatocellular carcinoma who have failed or are intolerant to first- and second-line therapies [12]. Additional dosimetry studies have recently demonstrated that AM RF EMF are delivered from head to toe in patients receiving treatment administered by means of an antenna placed in their mouth with similar SAR in the brain and the liver [13]. Therefore, AM RF EMF could be ideal for treating brain metastatic disease which has limited treatment options available. In this study, we examined the effect of BCF and its mechanistic action in treatment of brain metastasis of breast cancer.

In this study, we demonstrate that BCF treatment significantly suppresses the onset of metastatic growth in the brain by activating cellular stress pathways. Notably, BCF inhibition was found to be mediated by the activation of CACNA1H, which increased intracellular influx of calcium, leading to p38 MAPK activation. We also found that BCF reduces the self-renewal of cancer stem cells (CSCs) through modulation of High Mobility Group AT-2 (HMGA2) gene expression. Furthermore, BCF suppressed angiogenesis in the tumour microenvironment by decreasing exosomal secretion of miR-1246. These results strongly demonstrate that BCF is a promising novel modality of treatment for breast cancer brain metastasis.

## 2. Materials and methods

### 2.1. Cell culture and reagents

Human breast carcinoma cell lines, T47D, BT-474, SKBR3 and MDA-MB231 (MDA231), MDA-MB-453 were purchased from American Type Culture Collection. MDA-MB231BrM2a (231BrM) was a kind gift from Dr. Massagué (Memorial Sloan-Kettering Cancer Center. SKBrM3 cell line was derived from parental SKBr3 cells through three rounds of *in vivo* selection [14]. SKBr3, SKBrM3, T47D, MDA231, 231BrM and MDA-MB-453 were cultured in DMEM medium supplemented with 10% FBS, streptomycin (100 mg/ml) and penicillin (100 units/ml). All cells were grown at 37 °C in a 5% CO2 atmosphere.

### 2.2. Animal experiments

All animal experiments were conducted in compliance with the protocol approved by the Laboratory Animal Care and Use Committee of Wake Forest University. Intracranial injections were performed as previously described. Briefly, 5–6 weeks SCID mice (Harlan) were anesthesised by intraperitoneal injection of ketamine/xylazine (90–120/7–10 mg/kg). The hair was removed using clippers (ChroMini chordless clippers, Harvard apparatus) followed by shaving the hair (2 mm breadth and 8 mm length) with the razor. The area of incision was cleaned using sterile cotton swab. Then the mouse was positioned into a Kopf stereotactic frame. With the mouse secured in the stereotactic frame, we swabbed the forehead (between eyes back to ears) with betadine *via* sterilised cotton swab, and then used a scalpel to make a 5–6 mm caudal-rostral incision slightly to the right of midline while stretching skin with thumb and forefinger and avoiding the prefrontal sinus. We then used the wood end of cotton swab to scrape away fascial tissues covering the skull, and dry the skull well with the cotton end to

help locate midline and coronal sutures. A small burr hole was made by using sterilised Dremmel cordless drill (#76 drill bit) at the desired coordinates. A sterile 25-gauge needle attached to the syringe was introduced through the calvarium and into the brain at a depth of 4 mm. The cells were injected (volume of 5uL, 20,000 for SKBrM3 and 25,000 for 231-BrM cells). After one minute, the syringe was pulled up and a small amount of bone wax was applied to occlude the hole. The mouse was then removed from the frame and wound clips were used to close the skin. The tumour progression in the brain was monitored by bioluminescence imaging. Mice received Sham or BCF treatment one day after tumour implantation.

For intracranial injection of PDX2147 and PDX1435, PDXs were dissociated to single cell suspension using human tumour dissociation kit (Miltenyi Biotech). Dead cells were removed by using dead cell removal kit (Miltenyi Biotech) and 250,000 live cells were intracranially implanted to NOD/SCID mice. Tumour growth in brain was examined by MRI at day 30. Mice received Sham or BCF treatment one day after tumour implantation.

For intracardiac injections, 5–6 weeks SCID mice (Harlan) were injected into the left cardiac ventricle of the mice ($10^5$ SKBrM3 cells; $2 \times 10$ [5] 231-BrM cells). The cell growth and development of metastasis were monitored by bioluminescence imaging (BLI). Mice received Sham or BCF treatment one day after tumour implantation.

For combination of radiation and BCF, R2G2 mice were intracranially injected with 20,000 SKBrM3 cells labelled with luciferase and tumour growth was examined by BLI. When BLI reached $1 \times 10^6$, tumours were irradiated using precision X-Ray XRAD 320 Orthovoltage X-ray Unit with custom-made collimators (<5 mm diameter) and irradiation jigs housed in a shielded irradiator room. 40 gy (5 gy × 2 fractions/day for 4 days) radiation was delivered through positioning devices that ensured target-beam alignment with rodents positioned in the lateral or sternal recumbency position. Mice received Sham or BCF treatment after irradiation schedule was completed.

### 2.3. AM RF EMF exposure in vitro

Cell lines were exposed to 27.12 MHz radiofrequency electromagnetic fields using exposure systems designed to replicate clinical exposure levels. Experiments were conducted at an SAR of 30 and 400 mW/kg. Cells were exposed for three hours daily, seven days in a row. Cells were exposed to tumour-specific modulation frequencies that were previously identified by changes in pulse pressure in patients with a diagnosis of breast cancer or modulation frequencies never identified in patients with a diagnosis of cancer [15]. Specifically, the randomly chosen frequencies have been selected at random in the range of 500 Hz to 22 kHz, *i.e.* within the same range as the hepatocellular carcinoma-specific and breast cancer-specific frequencies. The only selection criterion within this range was for frequencies to be at least 5 Hz higher or lower than any hepatocellular carcinoma or breast cancer-specific frequency identified in patients with the corresponding diagnoses [15–17]. We have previously reported that the primary method for identification of tumour-specific frequencies is an increase in the amplitude of the pulse for one or more beats during scanning of frequencies [15]. Using the same method, we monitored variations in the amplitude of the radial pulse in thirty patients with a diagnosis of cancer, and did not observe any change in pulse amplitude during exposure to the randomly chosen frequencies.

### 2.4. In vivo treatment of amplitude-modulated radiofrequency electromagnetic fields

To replicate the dosimetric conditions resulting from intrabuccal administration of AM RF EMF *in vivo*, we designed and developed a small animal exposure system for AM RF EMF [18]. This exposure system allows for control of SAR levels in the same range as those generated by intrabuccal administration [18]. Mice were exposed to RF EMF amplitude-modulated at the previously published breast cancer-specific [16] frequencies 3 h each day till the experimental endpoint. The exposure system RF output was set for delivery of a SAR level of 255 mW/kg within the brain. This SAR was selected so that it is 1) within the range of previously demonstrated *in vitro* activity (30–400 mW/kg) [16] and 2) within the range of wbSAR1g and psSAR1g in patients receiving treatment with the TheraBionic device (1–352 mW/kg) [13]. All study protocols were approved by the Wake Forest Institutional Animal Care and Use Committee (IACUC).

### 2.5. RNA-sequencing and miRNA array

231BrM and SKBrM3 cells treated with Sham or BCF for 7 days ($n = 3$/sample) and RNAs were extracted using Direct-zol™ RNA MiniPrep Plus kit (Zymo Research, Catalog number: R2072). The alignment and quality control of RNA-Seq data followed the pipeline developed by the NCI's Genomic Data Commons (GDC, https://gdc.cancer.gov/). For exosomal miRNA isolation, exosomes were collected from SKBrM3 cells treated with Sham and EMF for 7 days and miRNAs were extracted using miRNeasy Micro Kit (Qiagen, Catalog number: 217084). Expression profiling of miRNA was performed by using the human miRNA chip (GeneChip miRNA 1.0 Array). Clustering and its visualization were performed using Cluster3.0 and TreeView.

### 2.6. [$3^H$]thymidine incorporation assay

Growth inhibition (GI) was assessed in breast cancer cells exposed to breast-specific modulation frequencies as previously described [19]. Briefly, cells were treated with the frequencies for 7 days, 3 h every day. At day 7, cells were washed, $^3$H thymidine (Amersham) was added, and cells were incubated for 4 h. After 4 h incubation, cells were washed with ice-cold PBS, fixed for 1 h with 95% methanol, rewashed in PBS, and lysed with 0.2 N NaOH. $^3$H thymidine incorporation was measured using the Beckman Coulter scintillation counter.

### 2.7. MTS Cell proliferation assay

Five hundred cells/well were seeded into 96-well plates in regular growth medium. Cell viability was measured by the MTS assay according to the manufacturer's recommendations (Promega) at indicated days.

### 2.8. Colony formation assay

SKBrM3 and SKBrM3-RR cells were treated with Sham or BCF for 7 days. At day 7, cells were seeded in 6-well plate (500 cells/well), exposed to 5 Gy of radiation and allowed to grow in a regular medium. At day 7 (after irradiation), the colonies were fixed with ethanol for 30 min, stained with Crystal Violet (CV) for 20 min and then the number of colonies was counted manually.

### 2.9. Flow cytometric analysis

For CSC analysis, cells were collected after 7 days of BCF or Sham treatment, washed with PBS, and incubated with CD44-APC and ESA-PE for 20 min followed by examining marker positive population ($CD44^{high}$,$ESA^{high}$) using BD Accuri. For calcium assay, Fluo-4 dye was added to the media of cells that were previously exposed to Sham or BCF for 2 h and 30 mins. After Fluo-4 addition, cells were exposed to Sham or BCF 30 mins. Cells were kept at room temperature for 30 min, washed twice with HBSS, scraped off from dish, dissociated by gentle pipetting, and ran on BD Accuri.

### 2.10. Sphere-forming assay

Cells were plated (200 cells/well) in 96-well ultra-low attachment plates (Corning) with DMEM/F12 supplemented with 2% B27 (Invitrogen), 20 ng/ml EGF (Sigma-Aldrich), and 4 μg/ml insulin (Sigma-Aldrich). The number of mammospheres was counted at Day 7, and data were represented as the means ± SEM.

### 2.11. Quantitative RT-PCR (qRT-PCR) analysis and PCR array

Total RNA was isolated from the cells and reverse transcribed. The cDNA was then amplified with a pair of forward and reverse primers to validate the results of microarray and PCR array. The thermal cycling conditions consisted of an initial denaturation step at 95 °C for 1 min followed by 35 cycles of PCR using the following profile: 94 °C for 30 s, 60 °C for 30 s, and 72 °C for 30 s.

CACNA1g (CAV 3.1)-Forward primer: 5′ CTT ACC AAC GCC CTA GAA ATC A 3′.

CACNA1g (CAV 3.1)-Reverse primer: 5′ GAT GTA GCC AAA GGG ACC ATA C 3′.

CACNA1h (CAV 3.2)-Forward primer: 5′ CAA GGA TGG ATG GGT GAA CA 3′.

CACNA1h (CAV 3.2)-Reverse primer: 5′ GAT GAG CAG GAA GGA GAT GAA G 3′.

CACNA1i (CAV 3.3)-Forward primer: 5′ GCC CTA CTA TGC CAC CTA TTG 3′.

CACNA1i (CAV 3.3)-Reverse primer: 5′ AGG CAG ATG ATG AAG GTG ATG 3′.

HMGA2 – Forward primer: 5′CAG CAG CAA GAA CCA ACC G 3′.

HMGA2 – Reverse primer: 5′TGT TGT GGC CAT TTC TAG GT3′.

miR-1246: Assay Id: 477881_mir; catalog # A25576.

### 2.12. Gene set enrichment analysis (gsea)

The Gene Matrix file (.gmx) was generated using top genes thate were significantly downregulated in BCF treated SKBrM3 cells. The Gene Cluster Text file (.gct) was generated using a cohort of 710 patients as described previously [14], and patients were separated by their status of brain metastasis. The Categorical class file (.cls) was generated based on the brain-met status of each patient. The number of permutations was set to 1000.

### 2.13. Immunohistochemistry

Tissue sections from Sham or BCF treated mice were baked at 60 °C for 1 h, deparaffinized in xylene, and rehydrated and fixed in 10% neutral buffered formalin. The sections were stained with antibodies specific to human HMGA2 (Abcam) and mouse CD31 (Cell signalling) and visualised using the EnVision Plus system (Dako).

### 2.14. Western blotting

The cells were lysed and analysed by immunoblotting using antibodies specific for the following proteins: HMGA2 (Abcam; dilution 1:1000); α-tubulin (dilution 1:4000), p-p38 (dilution 1:2000), p38 (dilution 1:6000), p-eIF2α (dilution 1:500), JNK (dilution 1:1000), CAMKII (dilution 1:2000), p-CAMKII (dilution 1:200) and p-β-catenin (Ser552; dilution 1:500) (Cell Signalling Technology); and β-catenin (Santa Cruz biotechnology; dilution 1:1000).

### 2.15. Tube formation assay

Ninety six-well plates were coated with 50-mL growth factor-reduced Matrigel (BD) and incubated at 37 °C for 30 min to solidify. HBMECs ($2 \times 10$ [4] cells) were suspended in EGM-2 growth medium or serum-free conditioned medium from cancer cells, and they were seeded on top oggrowth factor-reduced Matrigel. For exosome treatment, exosomes were added to the EGM-2 media (100 μl total volume). After 6 h, photos were taken under a microscope, and the number of tubes structures per field was counted.

### 2.16. Exosome isolation

Exosomes were isolated by differential centrifugation as described previously. Cells were grown on extracellular vesicle-depleted 10% FBS DMEM media for 48 h and conditioned medium (CM) was collected for exosome isolation. CM was centrifuged at 300*g* for 30 min to remove cells. The supernatant was then centrifuged at 2000*g* for 20 min to remove apoptotic bodies. The supernatant from this step was further centrifuged at 16,500*g* for 20 min to remove microvesicles, and passed through 0.2 μM filter (Sarstedt, Numbrecht, Germany) to remove particles that are larger than 200 nm. Final centrifugation was done at 120,000*g* for 70 min to pellet down the exosomes. The isolated exosomes were analysed by electron microscopy with negative staining. Blood eoxsomes were isolated as previously described [20]. Briefly, 1 ml of serum was loaded to the qEV size exclusion colums (Izon), and exosomes were concentrated by centrifugation using the Amicon® Ultra-4 10 kDa column.

### 2.17. Knockdown and overexpression

Knockdown of $Ca_v$ T-type channels was accomplished using Human lentiviral shRNA plasmids in p-GFP-c-shLenti vector from Origene, CACNA1g (Locus ID 8913; Catalog # TL305680), CACNA1H (Locus ID 8912; Catalog # TL314243) and CACNA1I (Locus ID 8911; Catalog # TL314242). Lentivirus was derived from four different shRNAs for each individual gene, infected to cancer cells and knockdown was verified by qRT-PCR. The shRNA infected cells that showed highest knockdown were selected for further experiments. HMGA2 gene knockdown was performed using two human lentiviral shRNA plasmids in pLKO.1 vector from Sigma (Catalog number: TRCN0000021964 and TRCN0000021965). HMGA2 cDNA plasmid (Myc-DDK-HMGA2) was obtained from Origene (Catalog #: RC214629), and HMGA2 gene was subcloned to pSIN vector. pSIN-HMGA2 plasmid was then used to make the virus, which was infected to cancer cells and cells were further selected with puromycin. pCDNA3-β-catenin plasmid and control vector were obtained from Addgene and transfected to MDA-MB-231 and SKBr3 cells.

### 2.18. Statistical analysis

Results were reported as mean ± SEM. For *in vitro* experiments, the Student's *t*-test or one-way analysis of variance was applied. For *in vivo* experiments, group comparisons were performed using the nonparametric Mann-Whitney test or unpaired Student's *t*-test. Kaplan-Meier curve comparison was performed with the log-lank test.

### 2.19. Ethical statement

The Wake Forest Institutional Animal Care and Use Committee (IACUC) approved all animal experiments performed in this study. The patient was offered compassionate treatment with the TheraBionic P1 device, written informed consent was obtained, authorization to publish the patient's clinical data was granted and compassionate use was approved by the Ethics Committee of the Cabinet Médical de l'Avenue de la Gare 6, 1003 Lausanne, Switzerland. Additionally, a compassionate use request for use a non-conforming medical device was submitted to and approved by swissmedic: https://www.swissmedic.ch/swissmedic/en/home/medical-devices/market-access/exemptions-for-non-conforming-medical-devices.html Exemptions for non-conforming medical devices.

## 3. Results

### 3.1. Breast cancer-specific AM RF EMF (BCF) suppress growth of brain metastasis

The remarkable efficacy of BCF in a previous feasibility study [10] prompted us to examine the effect of BCF *in vivo*. We implanted Her2 positive breast cancer brain metastatic variant line SKBrM3 cells *via* intracardiac route in NOD-SCID mice followed by the treatment of animals with BCF for 3 h daily. As shown in Fig. 1A-C, BCF significantly reduced tumour metastasis in the brain and improved brain metastasis-free survival. However, treatment of mice with randomly chosen AM RF EMF (RCF) did not affect the tumour growth and metastasis-free survival of mice (Supplementary Fig. 1A-C). In addition, BCF decreased the tumour growth in brain when SKBrM3 cells were orthotopically implanted in the brain (Fig. 1D). We also implanted triple negative brain metastatic variant 231-BrM cells both systemically (Fig. 1E-F) and orthotopically (Fig. 1G), and found significant suppression of tumour growth and metastasis in the brain by BCF, similar to that observed for SKBrM3 cells. These results strongly indicate that BCF is able to suppress brain metastasis of breast cancer *in vivo*.

To accurately represent the cancer heterogeneity, we examined the effect of BCF using two patient derived xenograft (PDX) models. PDX2147 was established from the primary tumour of a patient with brain metastasis [21], and PDX1435 was established at our institution by implanting tumour from a brain metastatic lesion arising from

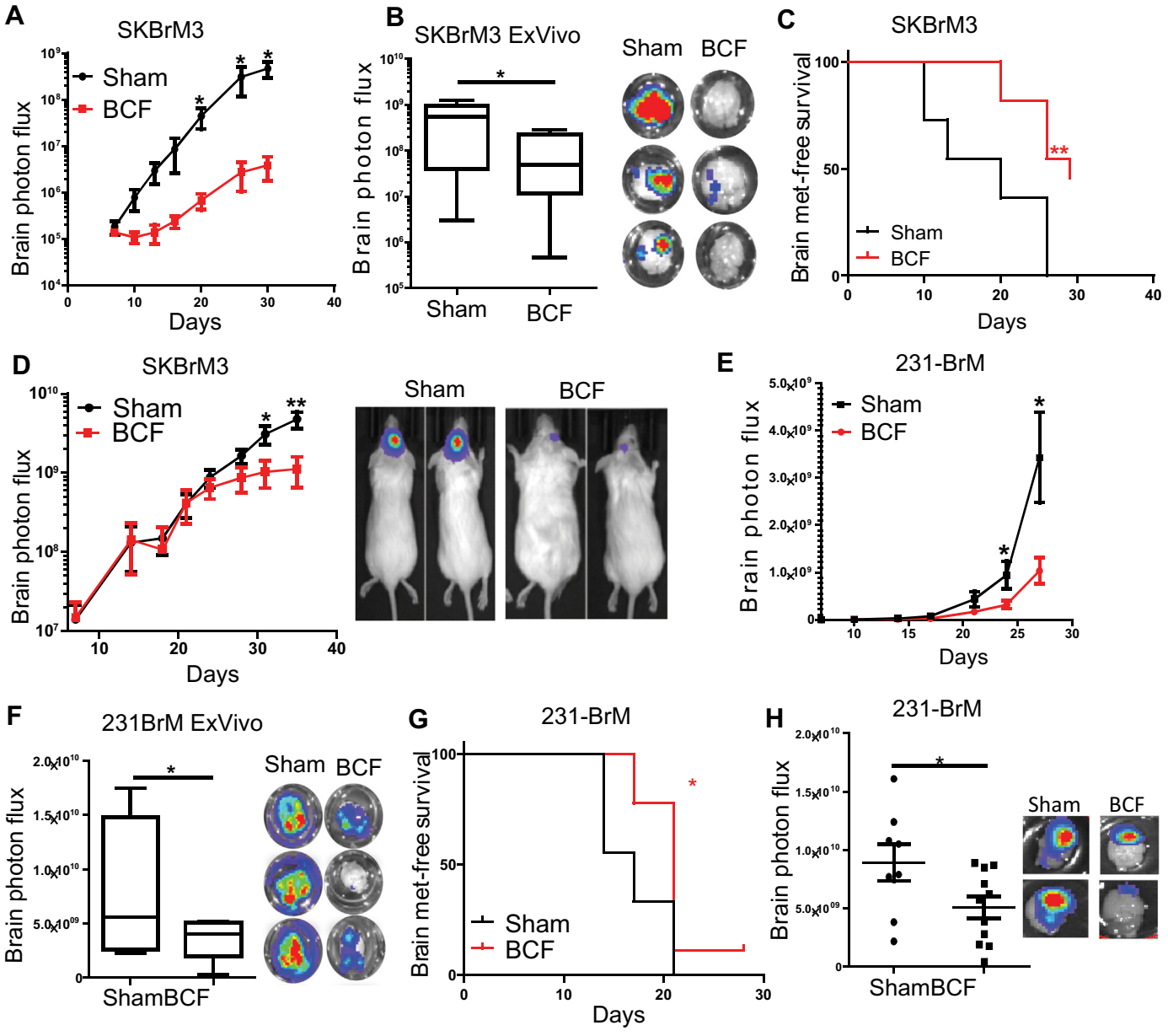


**Fig. 1.** Breast-specific BCF suppresses brain metastatic breast cancer cells *in vivo*. (A) SKBrM3 cells were injected through the intracardiac route followed by treatment of mice with Sham or BCF. Brain photon flux was examined by bioluminescence ($n = 11$/group). (B) *Ex vivo* bioluminescence was quantified for experiment performed in fig. A (C) Brain-metastasis free survival was plotted for Sham and BCF treated mice in fig. A. (D) SKBrM3 cells were implanted in the brain by intracranial injection and mice were exposed to Sham or BCF daily till day 36 ($n = 10$/group). Tumour growth was monitored by bioluminescence ($n = 8$/group). Inset panel shows representative bioluminescence images of Sham and BCF treated groups. (E) 231-BrM cells were intracardially implanted in mice followed by treating mice with BCF for 27 days ($n = 9$/group). Tumour growth in brain was quantified by bioluminescence imaging. (F) *Ex vivo* bioluminescence was quantified for experiment performed in fig. E (G) Brain metastasis-free survival was plotted for Sham and BCF treated mice in fig. E. (H) 231-BrM cells were intracranially implanted in brain and mice were treated with Sham or BCF everyday till day 42. Tumour growth in the brain was quantified *ex vivo* by using bioluminescence imaging at day 42. Right panel shows representative *ex vivo* bioluminescence image for BCF and Sham group. *, *P*-value<.05 and ** P-value<.01.

triple negative breast cancer. PDXs were dissociated into single cell suspension and implanted into the brain of NOD/SCID mice. As shown in Fig. 2A-C and supplementary fig. 1D-E), BCF significantly reduced PDX growth in brain. These promising results led us to offer compassionate treatment to a patient with metastatic disease (Supplementary Fig. 1F). Importantly, BCF daily treatment resulted in the remarkable reduction of the brain metastasis as shown in the MRI (Fig. 2D-G). The effect of treatment persisted for 11 months, while the average survival rate of patients with brain metastasis is <4 months [22].

### 3.2. Tumour suppressive effect of BCF is mediated through T-type voltage gated calcium channel and p38 MAPK signalling

To examine the direct inhibitory effect of BCF *in vitro*, we treated 231-BrM and SKBrM3 cells with BCF daily for 3 h, the same exposure

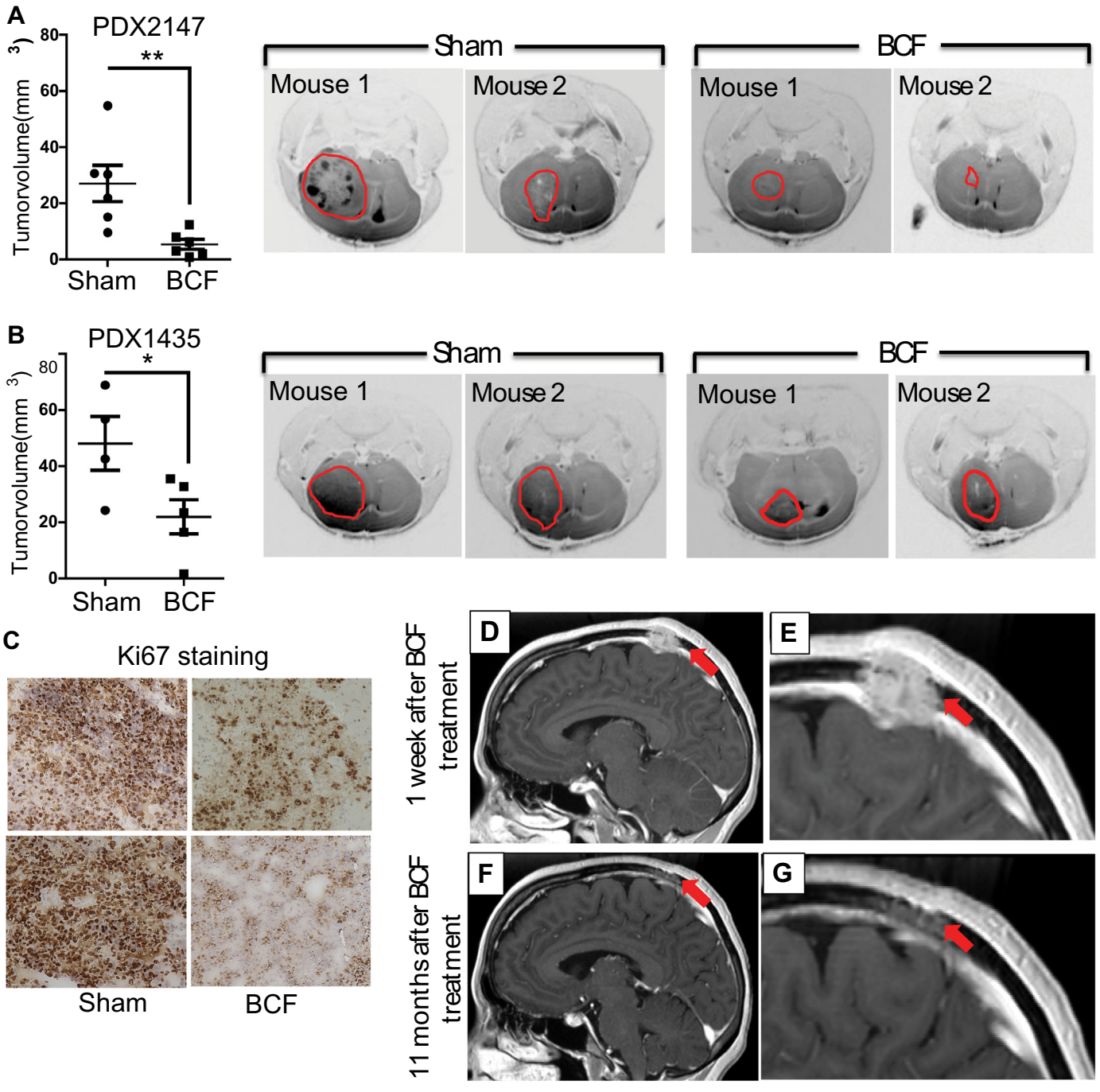


**Fig. 2.** Effect of BCF in a brain-met PDX model and patient. (A) PDX2147 was dissociated into single cell suspension and 250,000 live cells were intracranially injected into the brain. Mice were treated with Sham ($n = 6$) or BCF (n = 6) for 30 days and MRI was performed to visualise and quantify the tumour volume. (B) PDX1435 was implanted in brain treated with Sham ($n = 4$) or BCF ($n = 5$) and quantified for tumour volume at day 30 as in A. (C) Brain tumours from PDX2147 were stained for Ki67 expression by immunohistochemistry. (D-G). Treatment of brain metastasis (metastatic calvarial lesion) arising from triple negative breast cancer. Serial T1-weighted post-contrast magnetic resonance imaging (MRI) in sagittal plane, including magnified views (E and G) dated 8/30/2013 (D and E) and 8/8/2014 (F and G). Images D and E demonstrate an aggressive ovoid 2.7 cm (AP) x 3.5 cm (ML) x 1.6 cm (CC) enhancing mass centered in the parasagittal high left parietal calverium that extends into the scalp and intracranially, abutting and displacing the adjacent superior sagittal sinus. Images F and G demonstrate a marked interval decrease in size of the enhancing mass, now primarily localized in the diploic space and measuring 1.7 cm (AP) x 3.2 cm (ML) x 0.6 cm (CC) in size, with resolution of intracranial mass effect. AP = anteroposterior; ML = mediolateral; CC = craniocaudal; *, *P*-value<.05 and **, P-value<.01.

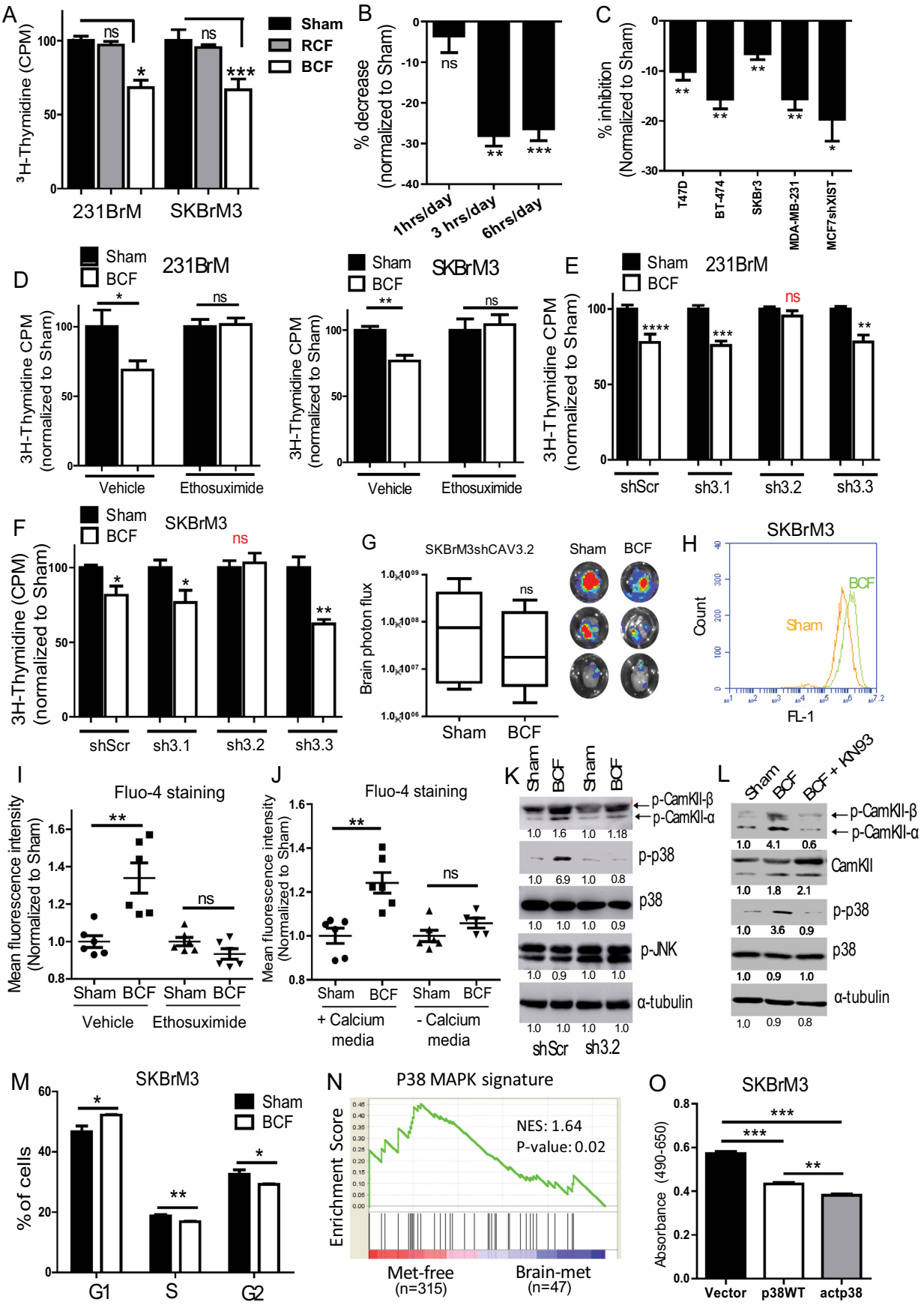
A
$^3$H-Thymidine (CPM)
Sham
RCF
BCF
231BrM
SKBrM3
B
% decrease (normalized to Sham)
1hrs/day
3 hrs/day
6hrs/day
C
% inhibition (Normalized to Sham)
T47D
BT-474
SKBr3
MDA-MB-231
MCF7shXIST
D
231BrM
3H-Thymidine CPM (normalized to Sham)
Vehicle
Ethosuximide
SKBrM3
E
shScr
sh3.1
sh3.2
sh3.3
F
G
SKBrM3shCAV3.2
Brain photon flux
H
Count
FL-1
I
Fluo-4 staining
Mean fluorescence intensity (Normalized to Sham)
J
+ Calcium media
- Calcium media
K
p-CamKII-β
p-CamKII-α
p-p38
p38
p-JNK
α-tubulin
shScr
sh3.2
L
BCF + KN93
CamKII
M
% of cells
G1
S
G2
N
P38 MAPK signature
Enrichment Score
NES: 1.64
P-value: 0.02
Met-free (n=315)
Brain-met (n=47)
O
Absorbance (490-650)
Vector
p38WT
actp38

time as in clinical and *in vivo* studies [15,17], for a period of 7 days. A significant reduction in cell proliferation was observed at day 7 when cells were treated with BCF but not by RCF (Fig. 3A). We have previously determined that 3 h and 6 h but not 1 h daily exposure for one week results in inhibition of hepatocellular cancer cell proliferation [16]. Similar inhibition was obtained for SKBrM3 cells treated with BCF 3 h or 6 h daily with no inhibition observed with 1 h daily (Fig. 3B). BCF treatment also decreased colony forming ability of brain metastatic cells (Supplementary Fig. 1G). In addition, BCF inhibited growth of highly brain-tropic cell lines; MCF7 and ZR-75-1 in which XIST expression was knocked-down [23] (Supplementary Fig. 1H). Similarly, the growth inhibitory effect of BCF was evident in multiple breast cancer cell lines (Fig. 3C). In contrast, treatment of normal breast cell, HMEC, brain-resident microglia, HMC3, and non-malignant immortalised breast cells, MCF10A, did not show any growth suppressive effect, providing strong support for the breast cancer-specific effect of BCF (Supplementary Fig. 1I). The decrease in cell proliferation was not associated with cell death, as BCF treatment did not induce apoptosis in brain metastatic breast cancer cells (Supplementary Fig. 1 J).

We previously reported that cellular calcium flux was affected by low energy electromagnetic fields, which were amplitude-modulated at specific frequencies [24–26]. In our study of hepatocellular carcinoma, we discovered that T-type voltage gated calcium channels (VGCC) mediate hepatocellular carcinoma specific AM RF EMF cell growth inhibition of hepatocellular carcinoma cell lines and xenografts [13]. Therefore, we treated breast cancer cells with ethosuximide, a pan T-type VGCC inhibitor, and found that the growth suppressive effect of BCF was significantly abrogated (Fig. 3D). We then knocked-down T-type channels by shRNAs (Supplementary Fig. 2A) and examined the effect of BCF. As shown in Fig. 3E and F, knock down of CACNA1H ($Ca_v3.2$ isoform), but not CACNA1G ($Ca_v3.1$ isoform) or CACNA1 ($Ca_v3.3$ isoform), rescued the suppressive effect of BCF in 231-BrM and SKBrM3 cells. Knockdown of CACNA1H also abrogated *in vivo* inhibitory effect of BCF when cells were injected systemically (Fig. 3G). T-type channels are transiently activating plasma membrane channels that mediates calcium influx upon their activation [27]. Concomitantly, BCF treatment induced intracellular calcium influx, which was nullified in the presence of ethosuximide or when cells were cultured in calcium free media, indicating that BCF mediates calcium influx through T-type channels (Fig. 3H-J). This effect was specific to BCF as RCF treatment showed no effect in intracellular calcium level (Supplementary fig. 2B). Additionally, treatment with BCF did not alter intracellular calcium level of normal glia (HMC3) and muscle cells (Supplementary 2C). These results suggest that BCF specifically target breast cancer CACNA1H resulting in calcium influx restricted to the breast cancer cells.

Intracellular and extracellular calcium level is precisely controlled in cells and it is involved in regulating various pathways as well as in stress signalling [28]. Calcium influx disrupts intracellular calcium homeostasis and induces various stress-responding protein kinases, such as, p38 MAPK and JNK that are known to play a critical role in cell cycle arrest and growth inhibition [29,30]. Therefore, we examined signalling from these pathways by immunoblot analysis after BCF treatment, and found that phospho-p38 was indeed significantly increased upon BCF treatment, suggesting that calcium influx activates stress response in BCF-treated cells (Fig. 3K). However, no significant change was observed in JNK expression (Fig. 3K). We also found that BCF, but not RCF, activated CAMKII, a known upstream kinase of p38 that is activated by calcium influx [31] (Fig. 3K and supplementary fig. 2D). When cells were treated with BCF in the presence of CAMKII inhibitor, KN93, p38 activation was rescued, suggesting that CAMKII is indeed the upstream kinase for p38 activation by BCF (Fig. 3L). Furthermore, BCF induced cell cycle arrest and elevated phosphorylation of the alpha subunit of translation initiation factor EIF2 (Fig. 3M and Supplementary Fig. 2E). We then examined the functional consequence of p38 MAPK activation in brain metastasis by Gene Set Enrichment Analysis (GSEA). p38 MAPK signature was found to be highly enriched in patients without metastasis when compared to patients with brain metastasis (Fig. 3N). To further validate this clinical finding, we expressed wild type and constitutively active p38 (D176A) in SKBrM3 cells (Supplementary Fig. 2F). As shown in Fig. 3O, stable expression of both wild type and active p38 strongly suppressed the cell growth of SKBrM3 cells. To examine whether p38MAPK pathway is activated by calcium influx, we treated cells with Bay K8644, an agonist of L-type VGCC, for 3 h/day for 7 days. Bay K8644 treated cells strongly activated p38 MAPK and reduced cell proliferation of SKBrM3 cells, which recapitulates the effect of BCF (Supplementary Fig. 2G and H). Collectively, these results suggest that BCF augments calcium influx through $Ca_v3.2$ channel and activates the p38 pathway to suppress cell growth.

### 3.3. BCF suppress cancer stem cell (CSC) through HMGA2

To further gain insight into the mechanistic action of BCF, we performed expression profiling analysis to identify differentially expressed genes following BCF treatment. As shown in Fig. 4A, nine genes were differentially up- or down-regulated commonly in both cell lines by the BCF treatment. Moreover, these genes downregulated by BCF were highly enriched in patients with brain-metastasis compared to the cohort of patient with no brain metastasis when examined by GSEA (Supplementary Fig. 3A). We then performed secondary screening of these 9 genes by analysing a cohort of 710 patients and examined their association with relapse-free survival (Fig. 4B and Supplementary Fig. 3B). Based on this criterion, the HMGA2 gene was selected for further investigation. Correlation of higher HMGA2 expression to worse outcome in breast cancer patients was further evident in METABRIC dataset (Supplementary Fig. 3C). Suppression of HMGA2 expression by BCF *in vitro* and *in vivo* was validated by qRT-PCR, western blot analysis and immunohistochemistry (Fig. 4C-E). Interestingly, HMGA2 level was found to be higher in patients with brain metastasis compared to patients with no metastatic disease or lung metastasis (Fig. 4F). Similarly, brain metastatic variants of breast cancer cells expressed higher level of HMGA2 than their parental cell lines, suggesting that the functional role of HMGA2 is linked to brain metastasis (Fig. 4G). HMGA2 is a transcription

**Fig. 3.** The inhibitory effect of BCF is mediated through $Ca_v3.2$ T-type channel and CAMKII/p38 MAPK pathway. (A) 231BrM and SKBrM3 cells were treated with Sham or random frequencies (RCF) or BCF for 7 days followed by thymidine incorporation cell proliferatin assay ($n = 5$/group). (B) SKBrM3 cells were treated with 1 h, 3 h and 6 h-per day for 7 days and cell proliferation was examined at day 7 by thymidine incorporation assay. (C) Various cell lines were seeded on 96-well plates at day 7 after Sham or BCF treatment, and cell proliferation was examined at day 1, 3 and 5 by MTS assay ($n = 8$/group). (D) 231BrM and SKBrM3 cells were exposed to Sham or BCF daily for 7 days in the presence of ethosuximide or vehicle, and cell proliferation was quantified by thymidine incorporation at day 7 ($n = 5$/group). Results are normalised to Sham group. (*E*-F) The T-type voltage-gated calcium channel subunit genes, $Ca_v3.1$, $Ca_v3.2$ or $Ca_v3.3$, were knocked down in 231BrM or SKBrM3 cells by shRNAs, and they were treated with BCF for 7 days followed by quantifying cell proliferation at day 7. (G) SKBrM3sh$Ca_v3.2$ cells were intracardially injected to NOD/SCID mice. At Day 30, *ex vivo* tumour signal in brain was quantified by bioluminescence. Right panel shows representative brain images. (H) Cells treated with Sham or BCF were stained with Fluo-4 calcium dye and the level of intracellular calcium level was examined using flow cytometry. The representative histogram is shown. (I) SKBrM3 cells treated with Sham or BCF in the presence of vehicle or ethosuximide were stained with Fluo-4-am dye and cytoplasmic calcium level was quantified by flow cytometry ($n = 6$/group). (J) SKBrM3 cells cultured in media with or without calcium and examined for cytoplasmic calcium as in I. (K) The expression of total and activated p38 and phosphorylated JNK was examined in 231BrM cells treated with Sham or BCF for 7 days by western blot. α-tubulin was used as a loading control. (L) 231-BrM cells were treated with Sham or BCF or BCF in the presence of KN93 (5 μM) and protein levels of phospho-CAMKII, total CAMKII, phopho-p38 and total p38 were examined by western blot. (M) SKBrM3 cells treated with Sham or BCF for 7 days were subjected to cell cycle analysis using FACS. % of population in G1, S and G2 phase are shown (n = 5/group). (N) Enrichment of biocarta P38MAPK signature in breast cancer patients with or without brain metastasis incidence was analysed by GSEA. (O) p38WT or p38 D176A (active mutation) gene or vector control was ectopically expressed in SKBrM3 cells using retrovirus and expression, and cells were seeded on 96-well plate ($n = 500$/well) and subjected to cell proliferation assay using MTS reagent at Day 5 ($n = 8$/group). *, *P*-value<.05, ** P-value<.01 and ***, P-value<.0001.

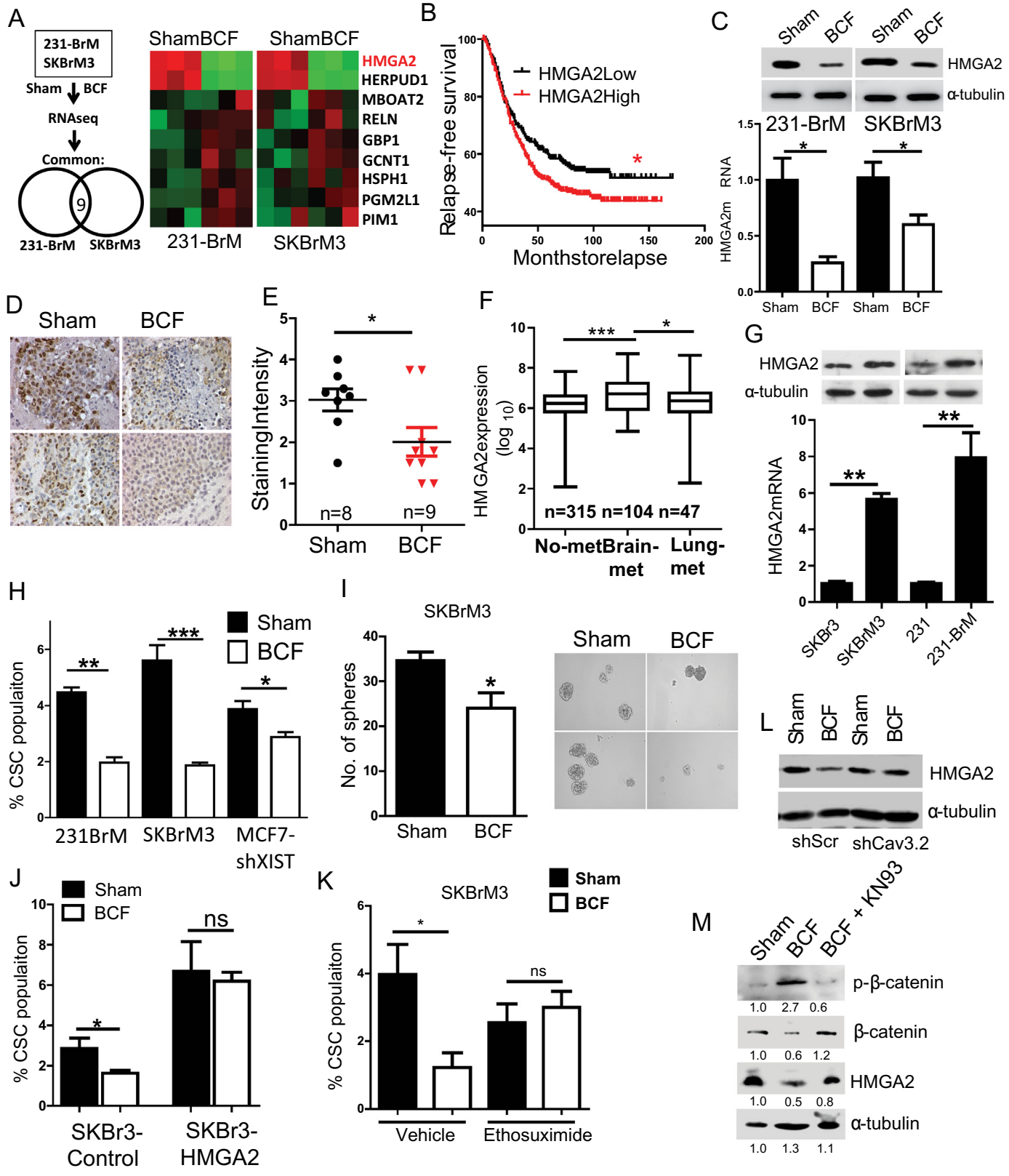


cofactor known to enhance tumourigenesis and metastasis of multiple cancer types by reprograming stem cells [32,33]. Therefore, we examined if BCF also affects the stem cell population. BCF treated cells indeed significantly reduced stem cell population and sphere forming ability of brain-tropic cancer cells without affecting stemness of neuron cells (Fig. 4H-I, Supplementary 3D). In addition, silencing HMGA2 in brain-tropic cells diminished stem cell population to an extent similar to BCF treatment (Supplementary Fig. 3E-F), while ectopic expression of HMGA2 in the parental cells, SKBr3 and MDA-MB-231, significantly increased the CSCs population (Supplementary Figs. 3G-H). Ectopic expression of HMGA2 also abrogated the suppressive effect on CSCs by BCF (Fig. 4J), suggesting that this effect on CSCs is mediated through downregulation of HMGA2. Additionally, the suppressive effect on HMGA2 and CSC was abrogated by ethosuximide treatment or $Ca_v3.2$

knockdown (Fig. 4K-L and Supplementary Fig. 3I—K). Previous reports suggest that calcium-influx activates CAMKII to phosphorylate and degrade β–catenin, which is a known upstream regulator of HMGA2 [34,35]. Therefore, we examined the possibility that calcium influx by BCF controls HMGA2 *via* β-catenin. Indeed, BCF strongly upregulated phosphorylated β-catenin level while decreasing the total β-catenin in CAMKII dependent manner (Fig. 4M). These results suggest that BCF suppress CSC population by decreasing HMGA2 expression through CAMKII-mediated β-catenin degradation.

### 3.4. BCF suppress exosomal miR-1246 expression

As shown in Fig. 2, the tumour suppressive effect of BCF is remarkably more prominent *in vivo* compared to its effect in cell based study *in vitro*. Therefore, we hypothesised that, in addition to its direct effect on tumour cells, BCF modulates cell-cell communication between tumour cells and stroma in the tumour microenvironment to amplify the suppressive effect *in vivo*. Exosomal vesicles or exosomes are known to be shed by tumour cells and carry components for cell-cell communication to promote tumour progression [36]. To examine the effect of BCF on exosomal RNA expression, we first isolated exosomes from SKBrM3 conditioned medium (CM) and confirmed the particle size by electron microscopy (Supplementary Fig. 4A). We then performed expression profile analysis of exosomal microRNAs from Sham- or BCF-treated SKBrM3 cells (Fig. 5A). We found that miR-1246 showed the highest extent of downregulation upon BCF treatment. The suppressive effect of BCF on miR-1246 was verified in both 231-BrM and SKBrM3 cells (Fig. 5B). In addition, the exosomes isolated from the blood of mice that were treated with BCF showed significantly diminished levels of miR-1246 (Fig. 5C). Consistent with these results, higher miR1246 expression was correlated with worse survival when TCGA dataset was examined (Fig. 5D). We also found that miR1246 expression is significantly higher in brain metastatic lesions compared to other metastatic sites (Fig. 5E). Similarly, serum level of miR-1246 was also elevated in patients with brain metastasis (Fig. 5F). In addition, the expression of both intracellular and exosomal miR-1246 was higher in brain tropic cells *in vitro* (Fig. 5G). Previous reports indicate that miR-1246 promotes tumour angiogenesis through intracellular and extracellular mechanisms [37,38]. Therefore, it is plausible that BCF suppresses angiogenesis in brain microenvironment by decreasing exosomal miR-1246 levels. To test this possibility, we treated human brain microvascular endothelial cells (HBMEC) with conditioned medium (CM) or exosomes prepared from BCF-treated brain metastatic cells. BCF treated CM or exosomes significantly decreased miR-1246 expression and tube-forming ability of HBMEC (Fig. 5H and supplementary 4B-C). To further verify the role of exosomal miR-1246 in angiogenesis, we prepared exosomes from MDA-MB-231 cells overexpressing miR-1246. Indeed, treatment with exosomes from 231-miR1246 cells increased the tube formation ability of HBMEC (Fig. 5I). Additionally, we ectopically expressed miR-1246 directly in HBMEC. These cells acquired higher tube forming ability concomitant with decreased expression of TSP2, which is a known target of miR-1246 (Supplementary Fig. 4D-E). We then performed immunohistochemical analysis for the brain tumours that were treated with BCF using mouse-specific anti-CD31 antibody to examine angiogenesis in brain tumours. As shown in Fig. 5J-K, tumours treated with BCF showed significant decrease in micro-vessel density, demonstrating that BCF decreases miR-1246 levels in exosomes to inhibit angiogenesis in brain microenvironment. In addition to its role in angiogenesis, miR-1246 was also reported to be involved in the Wnt pathway [39]. As HMGA2 and β-catenin are downstream components of Wnt pathway, we tested the possibility that BCF modulates miR-1246 expression through either β-catenin or HMGA2. Therefore, we performed a gain of function approach by expressing HMGA2 or β-catenin in 231 and SKBr3 cells. As shown in Fig. 5L and Supplementary Fig. 4F, ectopic expression of β-catenin, but not HMGA2, significantly elevated expression of miR-1246 in 231 and SKBr3 cells, indicating the role of β-catenin in regulation of miR-1246 expression. Collectively, these results demonstrate that BCF suppresses angiogenesis in the tumour microenvironment by suppressing β-catenin-miR-1246 signalling and that exosomal miR-1246 may serve as a potential biomarker of liquid biopsy to measure the effect of BCF in brain tumours.

### 3.5. Combination of radiation and BCF treatment suppress brain metastasis

Because radiation is the standard of care in the treatment of brain metastasis, and cancer stem cells are known to be involved in radiation resistance [6,40], we examined the effect of BCF on radio-resistant cell lines. We generated radiation resistant cell lines, 231BrM-RR and SKBrM3-RR (Fig. 6A). BCF treatment in these lines significantly suppressed their growth, CSC population, and colony formation ability, and this inhibition was rescued in the presence of Ethosuximide (Fig. 6B-F and Supplementary fig. 5A-B). This suppressive effect was accompanied by the downregulation of HMGA2 (Fig. 6D). We then examined the effect of the combination of BCF and radiation using the R2G2 mouse model. We found that BCF treatment combined with radiation significantly enhanced the anti-tumour effect compared to radiation alone, (Fig. 6G and supplementary 5B—C), suggesting a potential synergistic effect of radiation and BCF *in vivo*.

## 4. Discussion

Current therapeutic options for patients with brain metastatic disease are quite limited mainly due to the Blood Brain Barrier (BBB), which blocks the entry of therapeutic drugs into the brain, and ironically, tumour cells find the brain as a sanctuary. Radiation therapy approaches are the standard of care for brain metastasis. However, they have limited efficacy and recurrence is inevitable. Accordingly, the survival of patients with brain metastasis is dismal [41]. The robust growth inhibitory effect of BCF observed in this study has established its efficacy in the treatment of primary as well as recurrent metastatic tumours in the brain. The tumour and tissue specificity of BCF is further illustrated by the absence of antiproliferative effects in both HMEC and MCF10A in addition to the absence of antiproliferative effects on two hepatocellular carcinoma cell lines [16]. BCF mediated anti-proliferative effect on tumour cells through CACNA1H and the activation of p38 MAPK pathway. This demonstrates that low intensity RF EMF activate a specific transmembrane protein when modulated at specific frequencies, thus validating the hypothesis that BCF are demodulated by transmembrane

**Fig. 4.** BCF suppresses cancer stem cell population by decreasing HMGA2 expression. (A) Outline of RNA sequencing performed for 231-BrM and SKBrM3 cells exposed to Sham or BCF for 7 days (left panel). Expressions of 9 commonly up- or down-regulated genes are shown as a heat map on the right panel. (B) Overall relapse-free survival was examined by segregating breast cancer patients based on the HMGA2 expression level. Five GEO datasets were used to create a cohort with 710 patients. (C) HMGA2 expression was examined by western blot (upper panel) and qRT-PCR (lower panel) in 231-BrM and SKBrM3 cells after BCF treatment. (D-E) Brain tumour sections from Sham or BCF treated mice were examined for HMGA2 level by Immunohistochemistry, and the staining intensity was quantified. Representative images are shown in (E). (F) HMGA2 expression in patients with no metastasis (no-met), brain metastasis (Brain-met) and Lung metastasis (Lung-met) was examined in a combined cohort (see Methods section). (G) HMGA2 expression was examined in indicated cell lines by western blot (upper panel) and qRT-PCR (lower panel). (H) Cancer Stem Cells (CSC) population ($CD44^{high}/ESA^{high}$) was examined by FACS after treating 231-BrM, SKBrM3 and MCF7shXIST cells with Sham or BCF (n = 5/group). (I) Number of spheres was counted at day 7 after seeding SKBrM3 cells treated with Sham or BCF ($n = 6$/group). Representative pictures are shown in the right panel. (J) The CSC population in SKBr3 cells with or without overexpression of HMGA2 was quantified by FACS (n = 5/group). (K) CSC population was examined after treating SKBrM3 cells with Sham or BCF for 7 days (n = 5/group) in the presence of vehicle or ethosuximide. (L) 231BrM shScramble or $shCa_v3.2$ cells were treated with or without BCF for 7 days followed by western blot analysis to examine the level of HMGA2. (M) SKBrM3 cells were treated with Sham or BCF or BCF in the presence of KN93 (5 μM) and level of indicated proteins was examined by western blot. *, *P*-value<.05, **, P-value<.01 and ***, P-value<.0001.

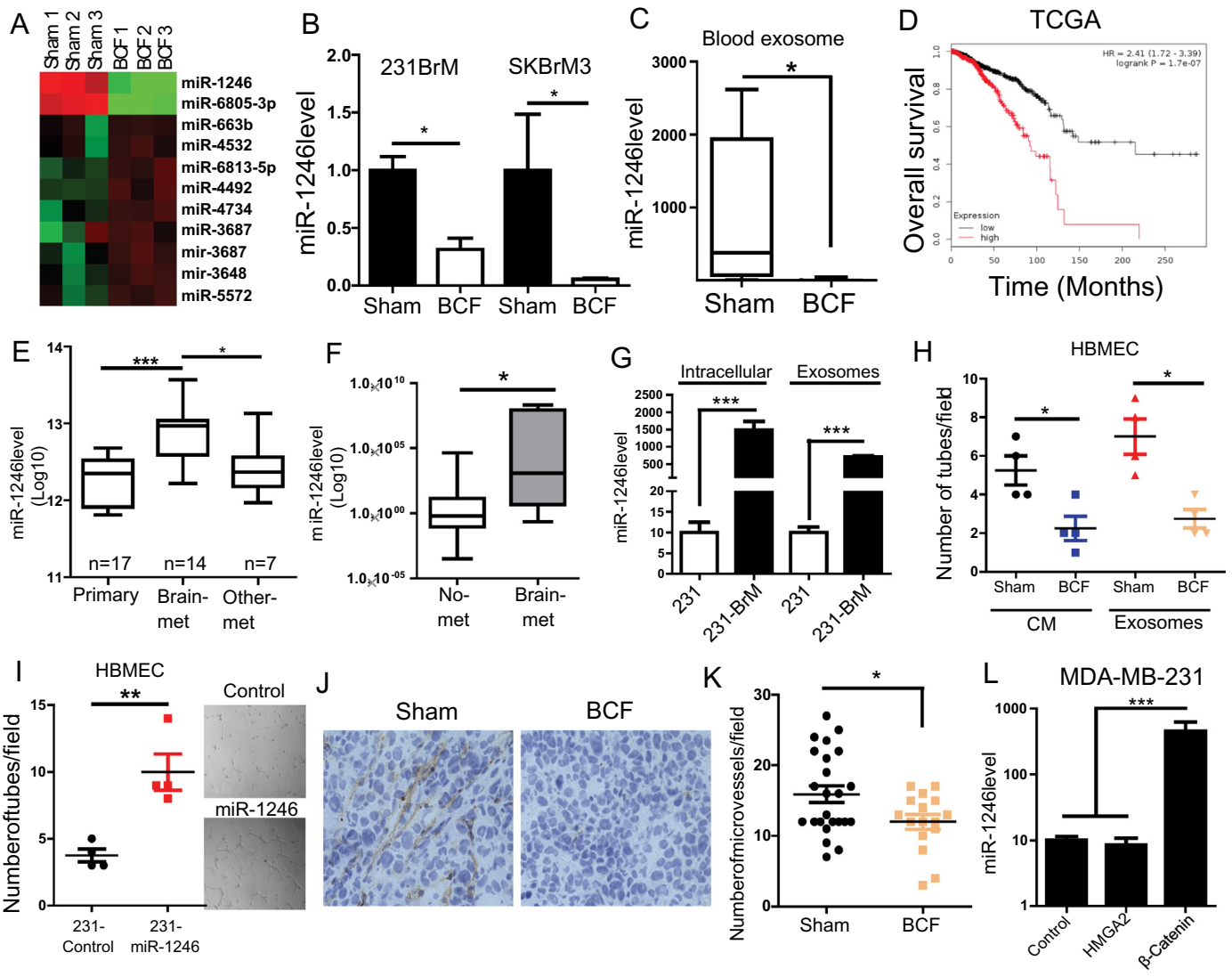


**Fig. 5.** BCF inhibits angiogenesis in brain tumour microenvironment. (A) Exosomes were isolated from SKBrM3 cells that were treated with Sham or BCF, and small RNAs were extracted and subjected to microRNA array analysis. Heat map shows the miRNAs that were significantly up- or down-regulated. (B) The expression level of miR-1246 in the exosomes prepared from 231-BrM and SKBrM3 cells that were treated with Sham or BCF for 7 days was examined by Taqman PCR. (C) Blood exosomes were isolated from mice treated with Sham or BCF and the expression level of miR-1246 was examined by Taqman qRT-PCR ($n = 5$ for Sham and $n = 8$ for BCF). (D) Relationship between miR-1246 expression and overall survival of patients in TCGA dataset was examined using kmplot website. (E) miR-1246 expression was examined in GEO37407 consisting of patients with no metastasis ($n = 17$), brain-metastasis ($n = 14$) and other metastasis including lymph node-, liver-, skin- and ovarian-metastasis. (F) miR-1246 expression was examined in serum exosomes isolated from patients with no metastasis ($n = 12$) or brain-metastasis (n = 8) patients. (G) miR-1246 expression in exosomes isolated from endogenous or exosomal fractions of MDA-MB-231 and 231-BrM were examined by Taqman qRT-PCR. (H) HBMEC were treated with CM or exosomes isolated from 231-BrM cells that were treated with or without BCF for 48 h, and the tube formation assay was performed by seeding cells in growth factor-reduced matrigel. Number of tubes were counted 6 h after the treatment with CMs. (I) Exosomes isolated from 231 or 231-miR-1246 cells were used to treat HBMEC cells for 48 h followed by seeding cells in growth factor reduced matrigel, and the number of tube formation were counted 6 h post seeding. (J-K) SKBrM3 tumours treated with BCF stained with mouse-specific CD31 antibody and the number of microvessel per 40× field was counted (K). Representative images are shown in J. (L) miR-1246 level was examined by Taqman PCR in 231 cells overexpressed with HMGA2 or β-catenin or control vector. *, P-value<.05, ** P-value<.01 and ***, P-value<.0001.

proteins, which act as an antenna [42,43]. We have shown that both $Ca^{2+}$ and CACNA1H are key mediators of the tumour cell response, capable of distinguishing breast cancer-specific AM RF EMF. Therefore, we propose that CACNA1H is selectively sensitive for tumour-specific AM RF EMF frequencies in epithelial malignancies. The notion that CACNA1H acts as the bioantenna for tumour specific AM RF EMF is strongly supported by our own findings showing that the same CACNA1H mediates the antiproliferative effects and repress CSCs in hepatocellular carcinoma following exposure to hepatocellular carcinoma-specific AM RF EMF [13].

We have previously reported that variation in pulse amplitude constitutes the primary method for identification of tumour-specific modulation frequencies [15], which have subsequently been shown to target cancer cell proliferation in a tumour and tissue-specific fashion [16]. CACNA1H is expressed in both endothelial cells and vascular smooth muscle cells of small arteries, which in turn directly affect pulse amplitude [44]. Hence, CACNA1H is the most probable link between the vascular system, crucial to the tumour-specific frequency identification process [15] and the anticancer effects observed *in vitro*, *in vivo* and in patients. Tumour-specific AM RF EMF appear to have a broad therapeutic window as tumour shrinkage was observed in humans [15,17], in human xenografts as presented in this report, and *in vitro* [16] at SARs ranging from 0.02 mW/kg to 400 mW/kg. In all conditions studied, treatment complies with the two standards for human exposure to RF EMF, the ICNIRP [45] and the IEEE [11]. Use of Pulsed Electromagnetic Fields (PEMF) has been associated with changes in $Ca^{2+}$ metabolism but the mechanism is mediated by L-type, not T-type VGCCs [46,47].

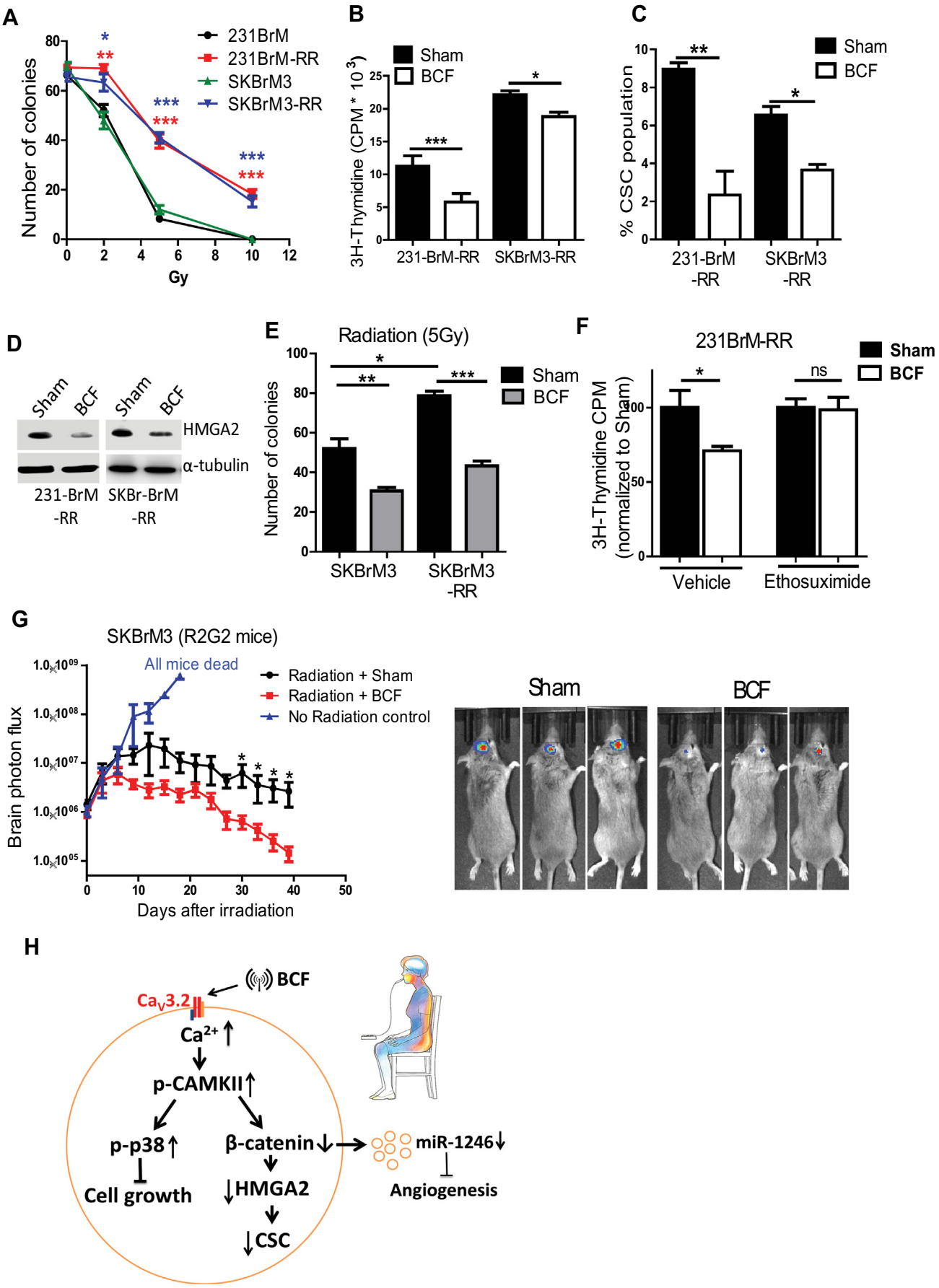
A
Number of colonies
231BrM
231BrM-RR
SKBrM3
SKBrM3-RR
Gy
B
3H-Thymidine (CPM * 10^3)
Sham
BCF
231-BrM-RR
SKBrM3-RR
C
% CSC population
Sham
BCF
231-BrM -RR
SKBrM3 -RR
D
Sham
BCF
Sham
BCF
HMGA2
α-tubulin
231-BrM -RR
SKBr-BrM -RR
E
Radiation (5Gy)
Number of colonies
Sham
BCF
SKBrM3
SKBrM3 -RR
F
231BrM-RR
Sham
BCF
3H-Thymidine CPM (normalized to Sham)
ns
Vehicle
Ethosuximide
G
SKBrM3 (R2G2 mice)
All mice dead
Radiation + Sham
Radiation + BCF
No Radiation control
Brain photon flux
Days after irradiation
Sham
BCF
H
BCF
Ca_V3.2
Ca2+
p-CAMKII
p-p38
Cell growth
β-catenin
HMGA2
CSC
miR-1246
Angiogenesis

VGCCs play major roles in tumour progression [48]. Specifically, T-type channels are known for both oncogenic and tumour suppressive functions in a tumour-type and context-dependent manner [49–51]. Our finding that AM RF EMF results in tumour inhibition through $Ca_v3.2$ T-type VGCC is consistent with a report in which drug treatment-induced calcium flux through $Ca_v3.2$ T-type VGCC inhibited breast cancer cell growth [52], suggesting that activation of this channel may play tumour suppressive role in breast cancer. However, studies in other tumour types suggest that inhibition of T-type VGCCs suppresses stem cell population and cell growth [50,53]. It should be noted that these studies used pan-T-type VGCC inhibitors and did not differentiate the isoform-specific effect in tumour inhibition. Calcium entry through T-type VGCCs are differentially regulated at each phase of cell cycle, and individual isoforms may play a specific role in a tumour-type dependent manner [54,55]. It is plausible that BCF alters the calcium oscillations from the $Ca_v3.2$ T-type channel at different stages of cell cycle to slow down transition from one stage to another. Therefore, BCF possibly disrupt breast cancer specific calcium oscillation to induce cell cycle arrest.

Multiple previous findings have revealed that exposure to EMFs can influence specific biological processes in cells such as cellular metabolism, morphology and differentiation [19]. Interestingly, some of these studies have shown that EMF treatment affects signal transduction pathways by regulating intracellular levels of c-AMP and calcium [49,56]. Other studies using mammalian models have shown that amplitude-modulated EMF affect calcium flux at specific frequencies, the so-called window effect, while unmodulated EMF do not result in any biological activity [42,43,57]. Similarly, exposure to pulsed electric field has been shown to increase calcium influx by decreasing plasma membrane integrity [58]. Our findings indicate that intracellular calcium flux through CACNA1H plays a crucial role in the suppressive effect of BCF. Furthermore, we also demonstrate that BCF induced calcium influx activates p38MAPK *via* CAMKII to inhibit cell growth. To our knowledge, this is the first report to identify CAMKII-p38 MAPK axis as a major player in EMF's biological effect on tumour cells (Fig. 6H). It was previously shown that p38 is activated by intracellular flux of calcium and induces cellular stasis or apoptosis [59,60]. However, we did not observe cell death in cells treated with BCF, suggesting that intermittent calcium flux through CACNA1H induced by BCF exposure activates p38 signalling only to mediate tumour suppressive effects without triggering cell death. It is also possible that CACNA1H functionally couples to putative microdomains to activate CAMKII-p38 signalling restricting calcium mobilisation to other cellular compartments.

We have also shown that BCF decreased the gene expression of HMGA2 to suppress cancer stem cell property of brain metastatic cells. The oncogenic function of HMGA2 was reported by several groups and mainly involves activation of stem cell programing in the tumour cells [32,33,61]. In fact, HMGA2 is known to be the downstream target of two major pathways that induce stemness, TGF-β- and Wnt – pathways [62,63] and a prognostic indicator of reduced relapse-free survival [64]. Therefore, it is conceivable that BCF reduces stem cell ability and cell proliferation *via* downregulation of HMGA2 gene expression. Importantly, our results suggest that the decrease in HMGA2 expression by BCF treatment was mediated through CACNA1H and CAMKII mediated β-catenin phosphorylation. The decrease in CSC explains the striking and long-lasting responses to BCF treatment for treatment-refractory metastatic patients which was observed in our previous feasibility trial [10].

Brain metastasis is a complex disease due to the unique environment of the organ. We and several other groups have shown that brain metastatic cells are molecularly rewired to communicate and modify brain microenvironment for tumour progression in the brain [14,65,66]. It was also reported that angiogenesis plays a prominent role in intracranial tumours arising from breast cancer, and inhibiting VEGF receptor tyrosine kinase suppressed tumour growth in the brain [67,68]. In fact, metastatic growth occurs in close proximity or by direct contact to the blood vessels in the brain [69]. In this report, we observed a significant decrease in exosomal miR-1246 level in BCF-treated cells. miR-1246 was previously found to promote tumour progression by augmenting angiogenesis [37]. Indeed, exosomes from BCF-treated cells suppressed angiogenic ability of brain microvascular cells in this study. Consistently, BCF treatment decreased $CD31^+$ microvessel density in tumours in the brain. Importantly, treatment of tumour bearing mice with BCF decreased the serum miR-1246 level, demonstrating the potential utility of this miRNA in predicting response to BCF in patients. Our results also indicate that brain-tropic variant cells shed higher levels of miR-1246 in exosomes. Therefore, miR-1246 may potentially serve as a biomarker of brain metastasis. Taken together, these results strongly suggest that miR-1246 orchestrate the angiogenic niche in the brain and that BCF disrupts miR-1246 signalling to suppress angiogenesis in the brain microenvironment. Last but not least, we provide the first evidence that the SAR level delivered by intrabuccal administration enables treatment of breast cancer brain metastasis.

Collectively, we have demonstrated that BCF effectively blocks the growth of breast cancer cells as well as breast CSCs through targeted activation of breast cancer cell CACNA1H resulting in increased intracellular calcium followed by activation of the CAMKII-p38 MAPK pathway and downregulation of HMGA2 expression. Therefore, BCF is a promising therapeutic approach to treat breast cancer metastatic disease, especially in the brain.

The results of our preclinical studies reported here and the example of a long-lasting response in a patient with brain metastasis together with the class IIa low risk designation of the device lay a strong foundation to test this promising novel approach in clinical trials that include patients with brain metastasis.

## Author contributions

SS and KW designed the study and wrote the manuscript. SS conducted experiments and acquired, analysed and interpreted the data. SYW performed PDX experiment. HJ treated cells and animals with BCF. FX and SYW derived the radiation resistant cells and performed intracardiac injections. SYW, DZ, YL, LMB assisted with intracranial injections and bioluminescence imaging. K Wu and AT isolated exosomes and performed tube formation assay. HWL assisted with Immunohistochemistry. PS, DJB, MDC and A Th provided various advices on experimental procedures. CTW and VK assisted with MRI image interpretation. RD assisted with study design, data analysis, data interpretation and review of manuscript. CB and BP provided the EMF exposure device, reviewed and edited manuscript and interpreted the data. KW supervised the study.

## Competing financial interests

Boris Pasche and Alexandre Barbault hold stocks in TheraBionic Inc. and TheraBionic GmbH. Carl Blackman has provided a loan to

**Fig. 6.** Combination treatment of radiation and BCF: (A) 231-BrM-RR and SKBrM3-RR cells were seeded into six-well plate and exposed to 2-, 5- or 10-Gy of radiation and number of colonies formed at Day 7 was counted. (B—C) 231-BrM-RR and SKBrM3-RR cells were treated with Sham or BCF for 7 days, followed by quantification of cell proliferation by thymidine incorporation assay (n = 6/group) (B) and CSC population by FACS (C). (D) HMGA2 expression was examined by western blot for 231-BrM-RR and SKBrM3 –RR cells after 7 days of exposure to BCF. (E) SKBr3 and SKBrM3 cells were treated with Sham or BCF for 7 days and 500 cells were seeded into each well of six-well plate followed by exposure to 5 gy of radiation. Number of colonies was counted at Day 7 (n = 6/group). (F) 231-BrM-RR cells were exposed to BCF or Sham daily for 7 days in the presence of ethosuximide or vehicle, and cell proliferation was quantified by thymidine incorporation at day 7 (n = 6/group). (G) SKBrM3 cells were injected in the brain of R2G2 mice. When bioluminescence signal reached 1*e [6], mice were irradiated with 40Gy (in 4 doses) followed by treating mice with Sham or BCF for 30 days. No irradiation mice were used as controls (n = 8/group) Representative images are shown in right panel. (H) Scheme of mechanistic action of BCF. *, P-value < .05, **, P-value < .01 and ***, P-value < .0001.

TheraBionic Inc. No other authors have any particular competing interests.

## Acknowledgements/funding

We thank Dr. Joan Massagué for providing the 231-BrM cell line. We also thank Dr. Michael T. Lewis for providing the PDX2147. This work was supported by NIH grant R01CA173499, R01CA185650 and R01CA205067 (to KW). The Tumour Tissue and Pathology Shared Resources, and Biostatistics/Bioinformatics Shared Resource are supported by the Comprehensive Cancer Center of Wake Forest University and, National Institutes of Health Grant (P30CA012197). The funding agency had no role in study design, data collection, data analysis, interpretation and writing of the report. The content is solely the responsibility of the authors and does not necessarily represent the official views of the National Cancer Institute.

## Appendix A. Supplementary data

Supplementary data to this article can be found online at https://doi.org/10.1016/j.ebiom.2019.05.038.

## References

[1] Greenberg H, Chandler W, Sandler H. Brain metastases. Brain tumors 1999;54:299–317.
[2] Mehta MP, Tremont-Lukats I. Radiosurgery for single and mutliple brain metastasis. Intracranial metastases: Current management strategies; 2004. p. 139–64.
[3] Eichler AF, Kuter I, Ryan P, Schapira L, Younger J, Henson JW. Survival in patients with brain metastases from breast cancer: the importance of HER-2 status. Cancer 2008;112(11):2359–67.
[4] Barnholtz-Sloan JS, Sloan AE, Davis FG, Vigneau FD, Lai P, Sawaya RE. Incidence proportions of brain metastases in patients diagnosed (1973 to 2001) in the metropolitan Detroit Cancer surveillance system. J Clin Oncol 2004;22(14):2865–72.
[5] Nussbaum ES, Djalilian HR, Cho KH, Hall WA. Brain metastases. Histology, multiplicity, surgery, and survival. Cancer 1996;78(8):1781–8.
[6] Andrews DW, Scott CB, Sperduto PW, et al. Whole brain radiation therapy with or without stereotactic radiosurgery boost for patients with one to three brain metastases: phase III results of the RTOG 9508 randomised trial. Lancet 2004;363(9422):1665–72.
[7] Lin X, DeAngelis LM. Treatment of brain metastases. J Clin Oncol 2015;33(30):3475–84.
[8] Meijer DK, Geesink HJ. Favourable and Unfavourable EMF frequency patterns in Cancer: perspectives for improved therapy and prevention. J Cancer Ther 2018;9(03):188.
[9] Geesink JH, Meijer DKF. Bio-soliton model that predicts non-thermal electromagnetic frequency bands, that either stabilize or destabilize living cells. Electromagn Biol Med 2017;36(4):357–78.
[10] Barbault A, Costa FP, Bottger B, et al. Amplitude-modulated electromagnetic fields for the treatment of cancer: discovery of tumor-specific frequencies and assessment of a novel therapeutic approach. J Exp Clin Cancer Res 2009;28:51.
[11] IEEE. IEEE standards for safety levels with respect to human exposure to radio frequency electromagnetic fields, 3 kHz to 300 GHz, IEEE C95.1–2005. New York: Institute of Electrical and Electronics Engineers; 2006.
[12] Goldberg P. TheraBionic P1 device receives European regulatory approval. Cancer Lett 2018 (Issue 31).
[13] Jimenez H, Wang M, Zimmerman JW, et al. Tumour specific amplitude-modulated radiofrequency electromagnetic fields induce differentiation of hepatocellular carcinoma via targeting Cav3.2 T-type voltage-gated calcium channels and Ca2+ influx. EBioMedicine 2019;44:209–24.
[14] Xing F, Liu Y, Sharma S, et al. Activation of the c-met pathway mobilizes an inflammatory network in the brain microenvironment to promote brain metastasis of breast Cancer. Cancer Res 2016;76(17):4970–80.
[15] Barbault A, Costa FP, Bottger B, et al. Amplitude-modulated electromagnetic fields for the treatment of cancer: discovery of tumor-specific frequencies and assessment of a novel therapeutic approach. J Exp Clin Cancer Res 2009;28(1):51.
[16] Zimmerman JW, Pennison MJ, Brezovich I, et al. Cancer cell proliferation is inhibited by specific modulation frequencies. Br J Cancer 2012;106(2):307–13.
[17] Costa FP, de Oliveira AC, Meirelles R, et al. Treatment of advanced hepatocellular carcinoma with very low levels of amplitude-modulated electromagnetic fields. Br J Cancer 2011;105(5):640–8.
[18] Capstick M, Gong Y, Pasche B, Kuster N. An HF exposure system for mice with improved efficiency. Bioelectromagnetics 2016;37(4):223–33.
[19] Zimmerman JW, Jimenez H, Pennison MJ, et al. Targeted treatment of cancer with radiofrequency electromagnetic fields amplitude-modulated at tumor-specific frequencies. Chin J Cancer 2013;32(11):573–81.
[20] Lobb RJ, Becker M, Wen SW, et al. Optimized exosome isolation protocol for cell culture supernatant and human plasma. J Extracell Vesicles 2015;4:27031.
[21] Zhang X, Claerhout S, Prat A, et al. A renewable tissue resource of phenotypically stable, biologically and ethnically diverse, patient-derived human breast cancer xenograft models. Cancer Res 2013;73(15):4885–97.
[22] Lin NU, Claus E, Sohl J, Razzak AR, Arnaout A, Winer EP. Sites of distant recurrence and clinical outcomes in patients with metastatic triple-negative breast cancer: high incidence of central nervous system metastases. Cancer 2008;113(10):2638–45.
[23] Xing F, Liu Y, Wu SY, et al. Loss of XIST in breast Cancer activates MSN-c-met and reprograms microglia via Exosomal miRNA to promote brain metastasis. Cancer Res 2018;78(15):4316–30.
[24] Blackman CF. ELF effects on calcium homeostatsis. Extremely low frequency electromagnetic fields; 1990.
[25] Blackman CF, Benane S, House D, Joines W. Effects of ELF (1–120 Hz) and modulated (50 Hz) RF fields on the efflux of calcium ions from brain tissue in vitro. Bioelectromagnetics 1985;6(1):1–11.
[26] Blackman CF, Benane SG, Kinney LS, Joines WT, House DE. Effects of ELF fields on calcium-ion efflux from brain tissue in vitro. Radiat Res 1982;92(3):510–20.
[27] Perez-Reyes E. Molecular physiology of low-voltage-activated t-type calcium channels. Physiol Rev 2003;83(1):117–61.
[28] Farfariello V, Iamshanova O, Germain E, Fliniaux I, Prevarskaya N. Calcium homeostasis in cancer: a focus on senescence. Biochim et Biophys Acta (BBA) Mol Cell Res 2015;1853(9):1974–9.
[29] Kuo PL, Chen CY, Hsu YL. Isoobtusilactone a induces cell cycle arrest and apoptosis through reactive oxygen species/apoptosis signal-regulating kinase 1 signaling pathway in human breast cancer cells. Cancer Res 2007;67(15):7406–20.
[30] Wright DC, Geiger PC, Han DH, Jones TE, Holloszy JO. Calcium induces increases in peroxisome proliferator-activated receptor gamma coactivator-1alpha and mitochondrial biogenesis by a pathway leading to p38 mitogen-activated protein kinase activation. J Biol Chem 2007;282(26):18793–9.
[31] Gardner OS, Dewar BJ, Graves LM. Activation of mitogen-activated protein kinases by peroxisome proliferator-activated receptor ligands: an example of nongenomic signaling. Mol Pharmacol 2005;68(4):933–41.
[32] Pallante P, Sepe R, Puca F, Fusco A. High mobility group a proteins as tumor markers. Front Med (Lausanne) 2015;2:15.
[33] Büssing I, Slack FJ, Großhans H. Let-7 microRNAs in development, stem cells and cancer. Trends Mol Med 2008;14(9):400–9.
[34] Kremenevskaja N, von Wasielewski R, Rao AS, Schofl C, Andersson T, Brabant G. Wnt-5a has tumor suppressor activity in thyroid carcinoma. Oncogene 2005;24(13):2144–54.
[35] Topol L, Jiang X, Choi H, Garrett-Beal L, Carolan PJ, Yang Y. Wnt-5a inhibits the canonical Wnt pathway by promoting GSK-3-independent beta-catenin degradation. J Cell Biol 2003;162(5):899–908.
[36] Wu K, Xing F, Wu S-Y, Watabe K. Extracellular vesicles as emerging targets in cancer: recent development from bench to bedside. Biochim et Biophys Acta (BBA) Rev Cancer Dec 1 2017;1868(2):538–63.
[37] Yamada N, Tsujimura N, Kumazaki M, et al. Colorectal cancer cell-derived microvesicles containing microRNA-1246 promote angiogenesis by activating Smad 1/5/8 signaling elicited by PML down-regulation in endothelial cells. Biochim et Biophys Acta (BBA) Gene Regul Mech 2014;1839(11):1256–72.
[38] Chen J, Yao D, Zhao S, et al. MiR-1246 promotes SiHa cervical cancer cell proliferation, invasion, and migration through suppression of its target gene thrombospondin 2. Arch Gynecol Obstet 2014;290(4):725–32.
[39] Chai S, Ng KY, Tong M, et al. Octamer 4/microRNA-1246 signaling axis drives Wnt/beta-catenin activation in liver cancer stem cells. Hepatol (Baltimore, Md) 2016;64(6):2062–76.
[40] Hardesty DA, Nakaji P. The current and future treatment of brain metastases. Front Surg 2016;3:30.
[41] Khuntia D. Contemporary review of the management of brain metastasis with radiation. Adv Neurosci 2015;2015.
[42] Adey WR, Bawin SM, Lawrence AF. Effects of weak amplitude-modulated microwave fields on calcium efflux from awake cat cerebral cortex. Bioelectromagnetics 1982;3(3):295–307.
[43] Blackman CF, Benane SG, Elder JA, House DE, Lampe JA, Faulk JM. Induction of calcium-ion efflux from brain tissue by radiofrequency radiation: effect of sample number and modulation frequency on the power-density window. Bioelectromagnetics 1980;1(1):35–43.
[44] Mikkelsen MF, Bjorling K, Jensen LJ. Age-dependent impact of CaV 3.2 T-type calcium channel deletion on myogenic tone and flow-mediated vasodilatation in small arteries. J Physiol 2016;594(20):5881–98.
[45] ICNIRP. Guidelines for limiting exposure to time-varying electric, magnetic and electromagnetic fields (up to 300 GHz). Health Phys 1998;74:494–522.
[46] Petecchia L, Sbrana F, Utzeri R, et al. Electro-magnetic field promotes osteogenic differentiation of BM-hMSCs through a selective action on ca(2+)-related mechanisms. Sci Rep 2015;5:13856.
[47] Li Y, Yan X, Liu J, et al. Pulsed electromagnetic field enhances brain-derived neurotrophic factor expression through L-type voltage-gated calcium channel- and Erk-dependent signaling pathways in neonatal rat dorsal root ganglion neurons. Neurochem Int 2014;75:96–104.
[48] Phan NN, Wang CY, Chen CF, Sun Z, Lai MD, Lin YC. Voltage-gated calcium channels: novel targets for cancer therapy. Oncol Lett 2017;14(2):2059–74.
[49] Buckner CA, Buckner AL, Koren SA, Persinger MA, Lafrenie RM. Inhibition of cancer cell growth by exposure to a specific time-varying electromagnetic field involves T-type calcium channels. PLoS One 2015;10(4):e0124136.
[50] Zhang Y, Cruickshanks N, Yuan F, et al. Targetable T-type calcium channels drive glioblastoma. Cancer Res 2017;77(13):3479–90.
[51] Jimenez H, Blackman C, Lesser G, et al. Use of non-ionizing electromagnetic fields for the treatment of cancer. Front Biosci (Landmark edition) 2018;23:284–97.

[52] Ranzato E, Magnelli V, Martinotti S, et al. Epigallocatechin-3-gallate elicits Ca2+ spike in MCF-7 breast cancer cells: essential role of Cav3.2 channels. Cell Calcium 2014;56(4):285–95.
[53] Sallan MC, Visa A, Shaikh S, Nager M, Herreros J, Canti C. T-type ca(2+) channels: T for targetable. Cancer Res 2018;78(3):603–9.
[54] Panner A, Wurster RD. T-type calcium channels and tumor proliferation. Cell Calcium 2006;40(2):253–9.
[55] Smedler E, Uhlen P. Frequency decoding of calcium oscillations. Biochim Biophys Acta 2014;1840(3):964–9.
[56] Buckner CA, Buckner AL, Koren SA, Persinger MA, Lafrenie RM. Exposure to a specific time-varying electromagnetic field inhibits cell proliferation via cAMP and ERK signaling in cancer cells. Bioelectromagnetics Apr 2018;39(3):217–30.
[57] Dutta SK, Subramoniam A, Ghosh B, Parshad R. Microwave radiation-induced calcium ion efflux from human neuroblastoma cells in culture. Bioelectromagnetics 1984;5(1):71–8.
[58] Morotomi-Yano K, Yano KI. Calcium-dependent activation of transglutaminase 2 by nanosecond pulsed electric fields. FEBS Open Bio 2017;7(7):934–43.
[59] Takeda K, Matsuzawa A, Nishitoh H, et al. Involvement of ASK1 in Ca2+−induced p38 MAP kinase activation. EMBO Rep 2004;5(2):161–6.
[60] Sosa MS, Avivar-Valderas A, Bragado P, Wen HC, Aguirre-Ghiso JA. ERK1/2 and p38alpha/beta signaling in tumor cell quiescence: opportunities to control dormant residual disease. Clin Cancer Res 2011;17(18):5850–7.
[61] Hammond SM, Sharpless NE. HMGA2, microRNAs, and stem cell aging. Cell 2008; 135(6):1013–6.
[62] Thuault S, Valcourt U, Petersen M, Manfioletti G, Heldin CH, Moustakas A. Transforming growth factor-beta employs HMGA2 to elicit epithelial-mesenchymal transition. J Cell Biol 2006;174(2):175–83.
[63] Wend P, Runke S, Wend K, et al. WNT10B/beta-catenin signalling induces HMGA2 and proliferation in metastatic triple-negative breast cancer. EMBO Mol Med 2013; 5(2):264–79.
[64] Wu J, Zhang S, Shan J, et al. Elevated HMGA2 expression is associated with cancer aggressiveness and predicts poor outcome in breast cancer. Cancer Lett 2016;376 (2):284–92.
[65] Xing F, Kobayashi A, Okuda H, et al. Reactive astrocytes promote the metastatic growth of breast cancer stem-like cells by activating notch signalling in brain. EMBO Mol Med 2013;5(3):384–96.
[66] Fidler IJ. The role of the organ microenvironment in brain metastasis. Semin Cancer Biol 2011;21(2):107–12.
[67] Monsky WL, Mouta Carreira C, Tsuzuki Y, Gohongi T, Fukumura D, Jain RK. Role of host microenvironment in angiogenesis and microvascular functions in human breast cancer xenografts: mammary fat pad versus cranial tumors. Clin Cancer Res 2002;8(4):1008–13.
[68] Kim LS, Huang S, Lu W, Lev DC, Price JE. Vascular endothelial growth factor expression promotes the growth of breast cancer brain metastases in nude mice. Clin Exp Metastasis 2004;21(2):107–18.
[69] Kienast Y, von Baumgarten L, Fuhrmann M, et al. Real-time imaging reveals the single steps of brain metastasis formation. Nat Med 2010;16(1):116–22.